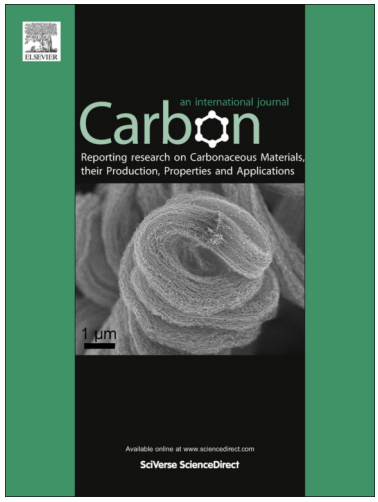

Defect-induced Fermi level pinning and suppression of ambipolar behaviour in graphene

Zakaria Moktadir, Shuojin Hang, Hiroshi Mizuta

PII: S0008-6223(15)00446-7
DOI: http://dx.doi.org/10.1016/j.carbon.2015.05.049
Reference: CARBON 9943

To appear in: *Carbon*

Received Date: 17 November 2014
Revised Date: 17 April 2015
Accepted Date: 17 May 2015

Please cite this article as: Moktadir, Z., Hang, S., Mizuta, H., Defect-induced Fermi level pinning and suppression of ambipolar behaviour in graphene, *Carbon* (2015), doi: http://dx.doi.org/10.1016/j.carbon.2015.05.049

Defect-induced Fermi level pinning and suppression of ambipolar behaviour in graphene

Zakaria Moktadir[a,*], Shuojin Hang[a], Hiroshi Mizuta[a,b]

[a] *Electronics and Computer Science, Faculty of Applied Physical Sciences, Southampton University, United Kingdom*
[b] *School of Materials Science, JAIST, Nomi, Ishikawa 923-1292, Japan*

Abstract

We report on systematic study of electronic transport behaviour of low-biased, disordered graphene nanowires. We reveal the emergence of unipolar transport as the defect concentration increases beyond 0.3% where an almost insulating behaviour is observed for n-type conduction whilst a metallic behaviour is observed for p-type conduction. The conductance shows a plateau that extends through the entire side above the Dirac point (n-branch) where the conductivity coincides with the minimum conductivity at the Dirac point. Raman spectroscopy and X-ray photoemission spectroscopy were used to probe the nature of the defects created by helium ion irradiation and revealed the presence of oxygen-carbon bonds as well as sp^3 configurations on the irradiated samples from C KLL Auger spectrum. The observed behaviour is attributed to oxygen groups created after the sputtering of carbon atoms by incident helium ions. These groups act as charge traps, pinning the Fermi level to the Dirac point.

1. Introduction

Graphene, a truly 2-dimentional material[1], has attracted enormous interest in the last decade and is listed as one of the major materials for post-CMOS era, according to the International Technology Roadmap for Semiconductors [2]. However, the absence of a band gap in graphene is a major hurdle towards its utilization in logic circuits for applications in electronics. Although the conductivity of graphene is tunable using electrostatic gating, the existence of a minimum conductivity [3, 4, 5] results in a finite "off" current and consequently a small on-off ratio is observed. Researchers have developed a wide variety of functionalization methods to open a band gap in graphene. A comprehensive review on graphene chemical functionalization can be found in reference 6. These modification techniques comprise fluorization[7, 8, 9, 10, 11, 12, 13], hydrogenation [14, 15, 16, 17, 18, 19, 20, 21, 22, 23, 24, 25, 26], oxidation[27, 28, 29, 30, 31, 32, 33],

*Corresponding author
Email address: zm@ecs.soton.ac.uk (Zakaria Moktadir)

chlorination[34, 35, 36, 37, 38, 39, 40] or functionalization with other chemical species[41, 42, 43, 44, 45, 46, 47, 48, 49]. Such functionalization has the effect of modifying the local electronic structure of carbon atoms in the hexagonal lattice, and functionalized sites can act as short range scatterers by modulating the local potential. The resulting random potential distribution in graphene sheet may induce localization phenomena[50, 51, 52, 53, 54, 55, 56, 57, 58, 59, 60, 61, 62] or it can result in the emergence of a band gap [15, 16, 49]. Band gap opening can also be achived without involving functionalization by applying an electric field across bilayer graphene sheet [63, 64]. Quasi-1D systems such as graphene nanoribbons or nanowires are of particular interest where edges strongly affect electronic states as they play a major role in the localization of carriers [51]. Beside the role played by edges, the localization of 2D electronic states can also occur by the deliberate introduction of structural defects in bulk graphene. A large amount of defects can be introduced in graphene by electron or ion bombardment for instance. A high level of disorder induced by electron irradiation was shown to possibly result in the formation of a two-dimensional amorphous carbon lattice[52]. Gallium ion irradiation on graphene flakes showed a structural transition from nano-crystalline graphene to amorphous carbon where the charge transport is dominated by variable range hoping process and where very short mean free path and localization lengths were observed [53]. In a recent report[61], it was shown that the introduction of defects in graphene narrow channels using lighter ions such as helium ions can be used to significantly alter graphene electronic properties. An on-off current ratio of 100 was found at room temperature. Scaling of the conductance was also observed showing an exponential decay as a function of the irradiated channel length implying that the transport is dominated by strong localization even at room temperature. This contrasts with the finding of reference 51 where edge disorder in narrow channels is responsible for strong localization.
In this paper we investigate transport properties of disordered graphene field effect nanowire devices. We found that as the disorder is increased, the Fermi level is pinned to the Dirac point and the ambipolar characteristic of graphene is suppressed whilst the conductance shows a plateau that extends through the entire side above the Dirac point (n-type) and the conductivity coincides with the minimum conductivity at the Dirac point. The minimum conductivity decreases with defect concentration pointing out towards the absence of zero energy modes in the defective samples. Despite the small on-off current ratio, the suppression of the ambipolar behaviour using helium ion irradiation is an essential requirement towards using irradiated graphene FETs in electronics.

2. Results and discussion

In figure 1 a sketch of the device is shown alongside a helium ion microscope (HIM) micrographs of typical two-terminal and multi-terminal devices considered here. Only the channel areas was subjected to irradiation with an accuracy less than 2 nm. The source and the drain contacts were not irradiated to avoid any variations in the contact resistance. In figure 2-A the room temperature

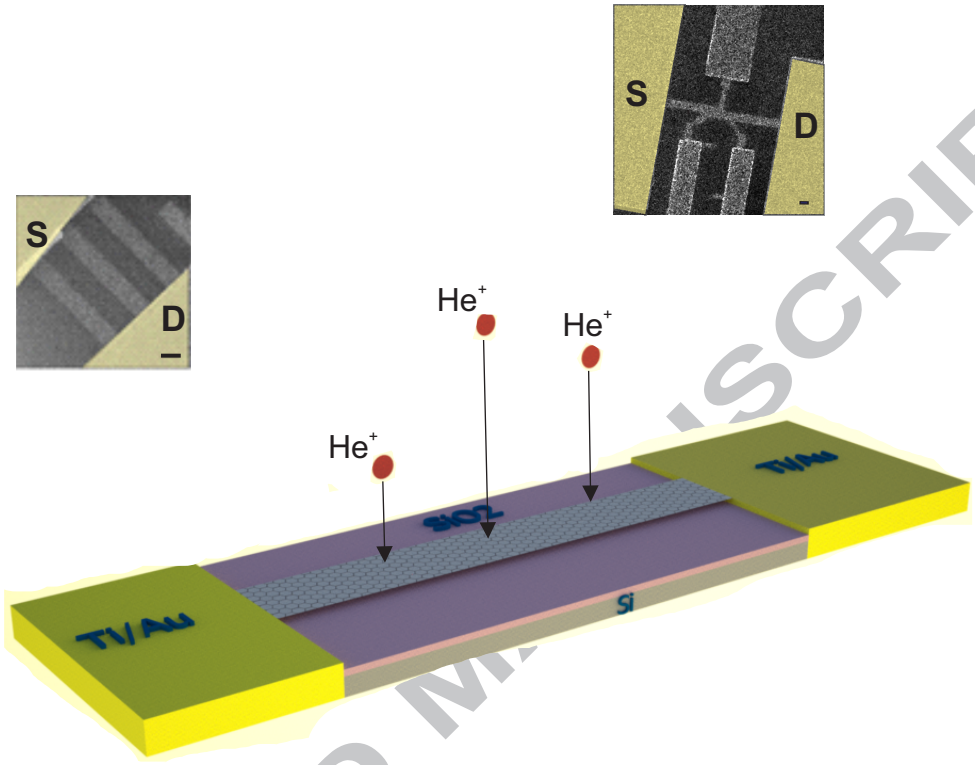

Figure 1: (a) Main panel: sketch of the fabricated device showing the channel, source and drain contacts. The channel is precisely irradiated with helium ions. The silicon substrate is used as a gate electrode whilst the silicon oxide layer ($\sim 300nm$) is used as a gate dielectric. Inset: the helium ion microscope micrographs of the fabricated two and multi-terminal devices used in this work, showing source, drain contacts and voltage probes. The scale bar is 200 nm for both insets.

I_d-V_d characteristics for six values of defect concentration n_d = 0.1 %-0.63 % in a two-terminal device are shown (for the defects concentration n_d derivation, see the Methods section). The I_d-V_d characteristics are linear for both, pristine and irradiated devices and show a clear absence of a transport gap in contrast with the findings in reference 61 where a transport gap was clearly observed in channels with similar width (200 nm) but shorter two terminal devices, at room temperature. The linearity is further confirmed by plotting the differential conductance dI_d/dV_d for the highest defect concentration n_d=0.63%, which is constant over the range of voltages used as shown in figure 2-C. The resistivity of the device increases with the defects concentration indicating an enhancement of carrier scattering by the created point defects. The defects were revealed by Raman spectroscopy which shows an increase in the D-peak as the irradiation dose is increased (see figure 5).

In figure 3-A we show the plot of the channel current versus the gate voltage

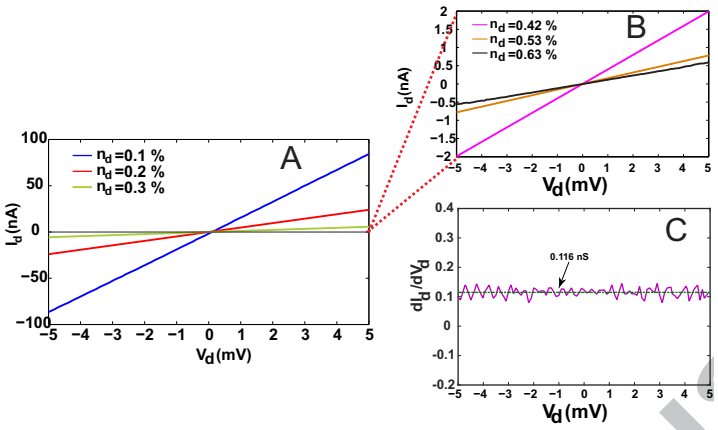

Figure 2: (A) Drain current-voltage characteristics of an irradiated channels which were 200 nm wide and 1 micron long. These characteristics were measured at different values of defect concentration as indicated. (B) A zoom-in of the characteristic near $I_d = 0$. (C) Differential conductance dI_d/dV_d for the highest defect concentration $n_d = 0.63$ %, indicating a conductance value of 0.116 nS.

(I_d-V_g curves) for non-irradiated and moderately irradiated graphene channels. In these plots the usual graphene characteristic is preserved showing an ambipolar behaviour and a neutrality point (NP). The conductivity varies linearly with the carrier concentration further away from the NP and shows a sub-linear behaviour at high values of V_g due to short-range scattering [5]. As expected, a decrease in the drain current is observed as the defect concentration is increased above 0.3%. Above this value the characteristics show a striking behaviour (figure 3-B): the devices no longer display the usual graphene Id-Vg curves but rather a flat characteristic above the NP (n-type conduction) and a superlinear behaviour below the NP (p-type conduction). For these devices, the NP corresponds to the value at which the polarity changes and the current starts to increase as the Fermi level is lowered into the valence band.

For the non-exposed device, one notices an asymmetry in the Id-Vg curves. This asymmetry is attributed to the large contact resistance, which dominates at high carrier concentration as clearly seen in the n-branch of the characteristic. In fact in our four point probe samples, the Id-Vg characteristics are perfectly symmetrical and become strongly asymmetrical when the samples are irradiated as shown in supplementary information (figure S1). Therefore the asymmetry in the characteristics is induced by defects.

In figure 4 the conductance I_d/V_d(in units of e^2/h) as a function of the defects concentration and the gate voltage is shown. From the semi-log plot we notice that the conductance decreases exponentially with the defect concentration.

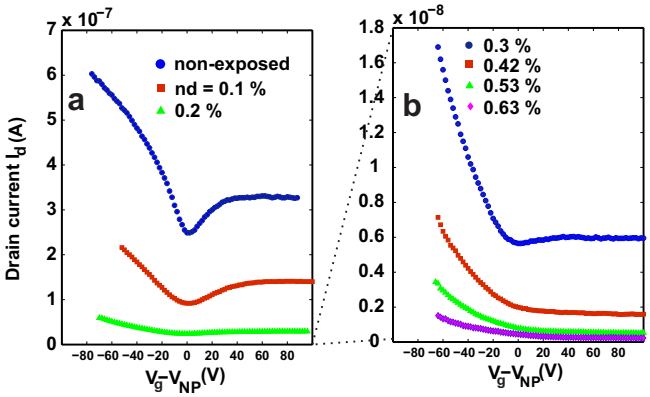

Figure 3: a) I_d-V_g curves for non-irradiated and moderately irradiated graphene nanoribbons. b) I_d-V_g curves for heavily disordered graphene ($n_d \geq 0.3\%$. Here the drain voltage is V_d= 5 mV.

We performed the same measurements on multi-terminal devices (see support-

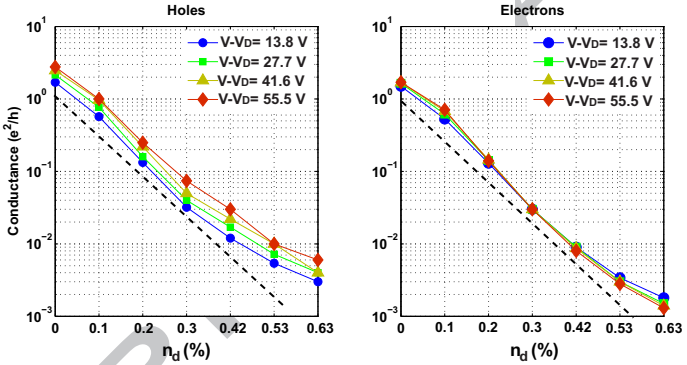

Figure 4: The exponential decrease of the conductance of a two-terminal device as a function of the defect density for holes and electrons.

ing information) and similar observations apply, that is the suppression of the ambipolar characteristic in irradiated channels. These multi-terminal devices were chosen to be wider (i.e. $w = 1\mu m$), to avoid the influence of the edges and thus assert that the observed behaviour is purely due to bulk defects created by He^+ bombardment.

To gain more understanding of the observed transport behavior and its correlation to the microscopic structure of disordered graphene, we performed Raman spectroscopy on irradiated graphene samples for similar defect concentrations (The laser excitation wavelength used was 532 nm). Before irradiation the D-peak which is indicative of disorder, is absent (see figure 5-A). As the defect concentration is increasing the prominence of D-peak is enhanced (at $\sim$ 1350 cm^{-1}), as expected. The ratio of intensities for the D-band and the G-band

decreases with the defect concentration. In line with previous works[65, 66], the evolution of the ratio ID/IG defines two stages called stage 1 and stage 2 disorders. The stage 1 disorder corresponds to low defect concentration where the ratio ID/IG $\simeq 1/L_D^2$, where L_D is the average distance between defects. The stage 2 disorder corresponds to ID/IG $\simeq L_D^2$ for high defect concentration. In terms of the average distance between defects $L_D = \sqrt{10^{14}/\pi n_d}$, this ratio is increasing for $L_D \leq 3$ nm, indicating a stage 2 disorder as shown in figure 5-B. The fit to the activation model[65] is also shown . The activation model predicts the following expression for the ratio I(D)/I(G):

$$\frac{I(D)}{I(G)} = C_A \frac{(r_A^2 - r_S^2)}{(r_A^2 - 2r_S^2)} \left(e^{\frac{-\pi r_S^2}{L_D^2}} - e^{\frac{-\pi (r_A^2 - r_S^2)}{L_D^2}} \right) + C_s \left(1 - e^{\frac{-\pi r_S^2}{L_D^2}} \right) \quad (1)$$

To increase the accuracy of the fitting procedure we added data for doses below 1×10^{15} cm^{-2} or for $L_D \geq 3$ nm. The parameter r_s corresponds to the radius of the structurally disordered area surrounding the impact point of an incident helium ion, whilst r_A is the radius of the area where the D-band transition occurs. The fit to equation 1 gives the following values for the parameters $C_A = 4.22 \pm 0.6$, $r_S = 0.96 \pm 0.13$ nm, $r_A = 2.24 \pm 0.16$ nm and $C_S = 0.97 \pm 0.05$.The Raman relaxation length for the resonant Raman scattering $l = r_A - r_S = 1.26 \pm 0.05nm$, which is consistent with the finding in reference 65 for graphene irradiated with Ar^+. The parameter C_A corresponds to the maximum value of the ratio I_D/I_G and its value derived here is smaller than the value found for graphene irradiated with Ar^+ for the same excitation wavelength[66].

An equally important quantity which is useful to probe the nature of defects is the ratio I(D)/I(D') [67]. In figure 5-C Raman intensities I(D) and I(D') (the D' peak is at 1600 cm^{-1}) are plotted as a function defect concentration n_d. The D-band intensity decreases with n_d whilst the D'-band is roughly constant for the range of n_d present in our samples. As a consequence the ratio I(D)/I(D') decreases with defect concentration as shown in figure 5-D. In stage 1, this ratio should not depend on the defect concentration but will only depend on the nature of defects[68]. The data shown in figure 5 is a clear indication that our irradiated samples are in stage 2 disorder [69]. Similar observations related to D and D' peaks emergence apply to fluorinated graphene [70]. One can estimate the average distance between defects L_D by examining the ratio I_D/I_G [70]. In our case, the clear distinction between the G and D' peaks for $n_d \geq 0.1$ % implies that samples are in the regime where I_D/I_G is increasing. For example for $n_d = 0.63\%$ the $I_D/I_G \simeq 0.7$ which gives an estimated L_D of 1.5 nm [65]. The decrease in the D-band intensity is consistent with theoretical predictions [71] where the maximum of I(D) is reached for a concentration of 6×10^{12} cm^{-2} before it starts decreasing for higher defects concentrations. The decrease in I(D) happens when the average length an electron/hole travels in between two scattering events with a defect becomes smaller than the average length an electron/hole couple travels before scattering with an optical phonon [71]. In this case, sp^2 groups become reduced and the rings become distorted.

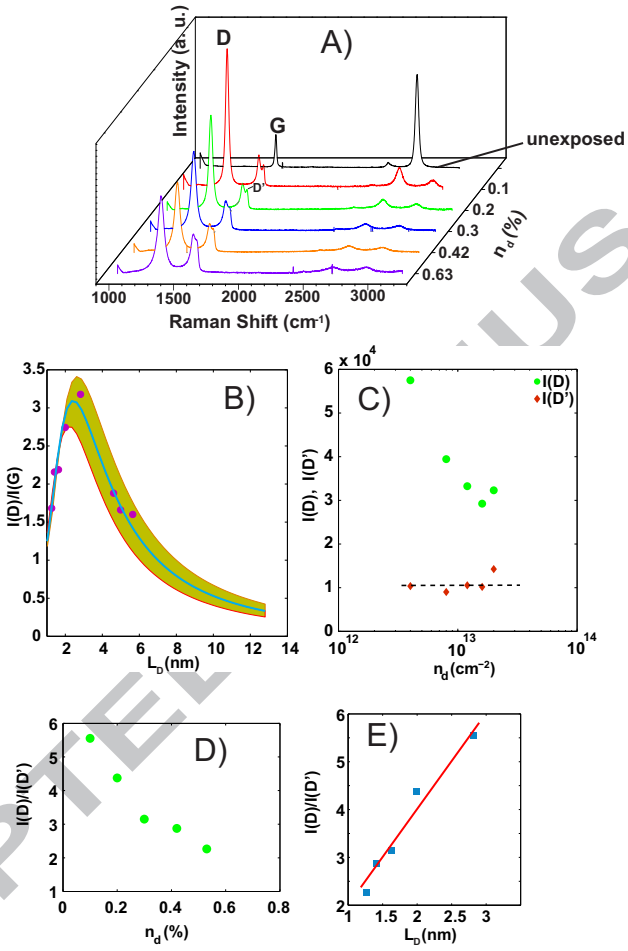

Figure 5: A) Raman spectrum versus defect concentration showing the emergence of the D-peak and the D'-peak as the concentration is increased. B) Plot of the ratio I(D)/(G) as a function of the average distance between defects L_D. The circles correspond to experimental data whilst the continuous bleu line corresponds to the best fit of the data to equation 1. The shaded area shows the uncertainty range corresponding to the parameters C_A, r_A, r_S and C_s determined form the fitting procedure. C) the plot of Raman intensities I(D) and I(D'), and in c) the ratio I(D)/I(D') are shown as a function of the defects concentration. In E) I(D)/I(D') is plotted versus the average distance between defects.

The strength of the D-peak is found to vary linearly with the average distance between defects according to the relation $I(D) \approx \alpha L_D \propto 1/\sqrt{n_d}$ (figure 5-D,E). Consequently, I(D)/I(D') $\propto 1/\sqrt{n_d}$ as I(D') is roughly constant over the range of defect concentrations present in our samples.
Contrary to stage 1 disorder where a correlation between the nature of defects and the ratio I(D)/I(D') can be drawn; in stage 2 however, it is still not clear how to relate the defects nature to the intensity ratio I(D)/I(D'). More systematic study is needed to clarify this correlation.

Another precise analytical method used to quantify disorder in graphene is the X-ray photoemission spectroscopy (XPS). In this work we performed XPS on irradiated graphene samples (for details see supporting information). First, a survey in the entire range of binding energy [0, 1200] eV was performed (see supporting information) to identify the different atomic species present in our samples besides carbon. No other elements were found apart from oxygen and silicon originating from the underlying SiO_2, although some oxygen may be present in the graphene sheet forming bonds with carbon. Figure 6 shows the C1s core level spectrum for different values of defect concentration.

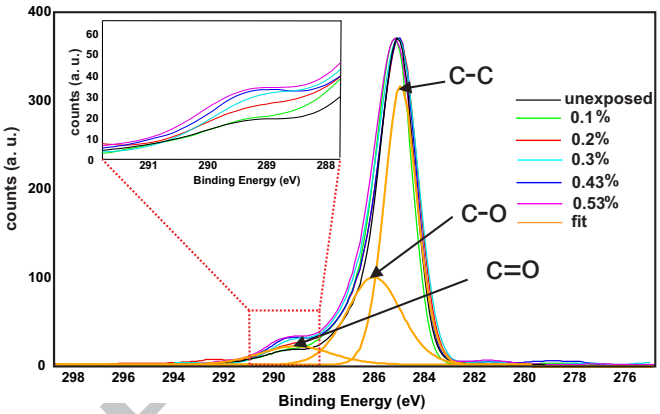

Figure 6: High resolution XPS spectrum of C1s core level for different values of defect concentration as indicated. The fit to one of the spectra (orange curve) shows the presence of three peaks at 284.4 eV, 286.5 eV and 288 eV. The inset shows the zoom-in of the area of the spectrum situated around the third component.

All the spectra show an asymmetric broad line and can be split into three components. The spectra were fitted to a convolution of Gaussian and Lorentzian functions. The major spectral component shows a slight shift in binding energy compared to the sp^2 line in graphite which is 284.4 eV [72, 73]. This shift might be attributed to charge transfer between the graphene sheet and the underlying oxide substrate. It was shown from previous works that the measured C1s core level binding energy in graphene depends on the underlying substrate and the difference can be few hundreds of meV [74, 75, 76]. Therefore we use the value for graphite i.e. 284.4 eV as a reference in all spectra measured for different defect concentration. The FWHM of the peak at 284.4 eV increases with defect concen-

tration indicating broadening. The sp^2 component persists even for the highest defect concentration $n_d = 0.63\%$, meaning that the graphene atomic structure is still preserved to a significant degree. For different defects concentrations, the other two components are roughly centered at 286 eV and 288.5 eV. These two peaks can be attributed to C-O and C=O groups respectively[77, 78, 79]. Similar observation were found in few layer graphene irradiated with electron [80] and irradiated graphite [72]. The sp^3 to sp^2 contents can be determined by the so-called the D-parameter which measures the distance between the maximum and the minimum in the carbon (C KLL) Auger electron first derivative[81, 82] spectrum. For pure graphite (pure sp^2) this parameter is 21 eV whilst it has a value of 13 eV diamond (pure sp^3)[82]. There is a linear relationship between the sp^2 to sp^3 ratio and the value of D[82]. We found a value of 18 eV for our He^+ irradiated graphene samples which did not vary significantly in the range of the defect concentrations used (0.1% - 0.63%). This indicated a ratio of sp^2 to sp^3 contents of 0.6 (see supporting information).
Helium ion sputtering of carbon atoms induces the presence of vacancies of different nature, although our XPS measurements couldn't resolve the location of peaks corresponding to vacancies due to the limited resolution of our XPS instrument. It was shown using density functional theory that the energy shift between the C1s peak location in graphene and the vacancies peaks is -0.64 eV, -0.49 eV and -0.34 eV for single vacancy, di-vacancy and Stone-Wales vacancy respectively[83]. These shifts were not resolved in our XPS spectrum. As the XPS measurements were performed after the samples were briefly exposed to air, these vacancies are more likely to be saturated with oxygen as shown in the XPS spectra.

The observed unipolar character of the conductance and the electron-hole asymmetry is very reminiscent to that predicted theoretically for H^+ adsorbates, whilst for OH^- absorbate the conductance shows an n-type behaviour[84]. However it is not clear if water molecules from the ambient provide the proton and the hydroxide group to an unsaturated dangling bond. This can be potentially probed by in-vacuum hydrogenation of irradiated graphene which has a passivation effect. More research is needed to clarify this. The presence of sp^3 structures revealed from the D-parameter can be attributed to out-of-plane deformation induced by defects as predicted theoretically for Stone-Wales defects[85] or by adsorbates that re-hybridize the sp^2 orbitals. In the present case, the main adsobates revealed by XPS are oxygen which form single and double bonds with carbon atoms.

In graphene, oxygen groups and vacancies act as short ranges scattereres and their presence induce a peak in the density of states at the Fermi level[86, 87, 88]. This particular type of defects is also called resonant scatterers as they strongly couple to graphene electronic states and thus scatter carriers very efficiently [89]. Covalently bonded adatoms and vacancies can also give rise to zero energy modes[90] (ZEMs) which produce a supermetallic regime by enhancing the Dirac-point conductivity above its minimum ballistic value $\sigma_{min} = 4e^2/\pi\hbar$[91].

Oxygen groups revealed by the XPS induce a local scattering potential at the sites where they are attached in the graphene lattice. As a consequence, resonances appear around E=0 in the density of states. The fact that in our samples the minimum conductivity (the conductivity was measured in multiprobe samples, see supporting information) decreases with defects concentration, suggests that these resonant states do not contribute to transport and are localised. This observation agrees with theoretical predictions from ab-initio calculations which show that single vacancies introduce localized trap states near the Dirac Point[92] which do not contribute to carrier transport. These localised trap states pin the Fermi level and explain the observed transport asymmetry in our samples. Below the Dirac point the Fermi level is free to move within the valence band triggering hole current as sketched in figure 7. For large defect concentration, the conductivity in the n-type channel coincides with the minimum conductivity and the minimum conductivity plateau usually seen in graphene extends to the whole n-side. The mechanisms by which this charge trapping occurs requires more attention. It is possible that the trap density is larger enough to overcome the available charge density induced by the gate voltage.

To uncover the existence of localisation phenomena, we have performed temperature-dependent conductivity measurements in other samples (see figure S6 in supporting information) which reveal that the conductivity is saturating at low temperature and does not show the $\exp\left(-(T_0/T)^{1/3}\right)$ dependence , in the range of defect concentration used. This rules out variable range hopping conduction mechanism in our samples and thus no strong localisation is present in the range of defects concentration considered. The defect concentration is not large enough to trigger the onset of strong localisation. The exponential decrease of the conductance with increasing defect concentration cannot be explained by strong localisation. This decrease might be due to the exponential collapse of the mobility because of the large density of scattering centres. More theoretical and experimental work is required to provide a quantitative interpretation.

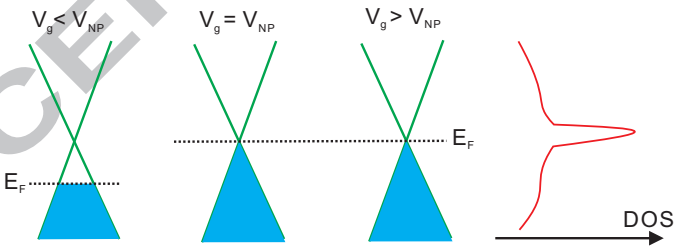

Figure 7: Sketch of the Fermi level pinning at the Dirac point. When the gate voltage is higher than the Dirac voltage, the conductivity is aligned with the minimum conductivity which determined by the defect-induced peak of the density of states (also shown) at the Fermi level. When the gate voltage is below the Dirac voltage, the Fermi level is unpinned and can freely move inside the valence band giving rise to hole conduction which changes with the Fermi level.

3. SUMMARY AND CONCLUSIONS

In conclusion we have systematically investigated the transport properties of field effect graphene devices irradiated with accelerated helium ions. The defect concentration was controlled by increasing the dose of the irradiated ions, and was in the range 0.2%-0.63%. As the defect concentration increases, an almost insulating behaviour is observed in n-type branch whilst a metallic behaviour is observed in the p-type branch. The conductance shows a plateau that extends through the whole side above the Dirac point (n-type branch) . This was a result of Fermi level pinning at the Dirac point which was induced by oxygen groups acting as charge traps. Raman spectroscopy and X-ray photoemission spectroscopy were used to probe the nature of the defects created by helium ion irradiation and revealed the presence of oxygen-carbon bonds as well as sp^3 configuration on the irradiated samples. The observed unipolar behaviour is an important step towards using graphene in logic circuits. However the question remains how to increase the on-current on the p-side and equally how to create an insulating behaviour on p-side which will allow complimentary logic operations. One solution is to decrease the channel length; this is an ongoing investigation.

METHODS

The graphene used in this work is obtained from mechanical exfoliation of highly oriented pyrolytic graphite (HOPG) on a 300 nm SiO2 layer sitting on a highly doped silicon substrate which is used as a back gate terminal. Single layer flakes were identified using both an optical contrast method and Raman spectroscopy [93, 94]. The Graphene nanowires were defined using ebeam lithography and oxygen plasma etching. This is followed by a second lithographic layer to deposit thermally evaporated Ti/Au (10 nm/80 nm) contacts using ebeam lithography and a lift-off process using a double layer of methylmethacrylate (MMA) and poly(methylmethacrylate) (PMMA) resists. The fabricated devices were baked overnight at 250 C to free the channels from contamination caused by the resist residue. The irradiation with helium ions He^+ was performed in high vacuum inside a helium ion microscope (Zeiss Orion) [95, 96, 97, 98, 99]. The acceleration voltage used was 30kV whilst the current was kept at 1 pA. To avoid variations of contact resistance, contacts were not exposed to the He+ beam and only graphene channels were irradiated. This was possible by the high precision patterning offered by the helium ion microscope, with a He^+ beam spot size of 0.7 nm. The channels were perfectly mapped using an embedded pattern generator. Experiments were performed on both two-terminal and multi-terminal devices at room-T. The measurement were performed immediately after each irradiation run, using an Agilent B1500 semiconductor analyser. The channels were exposed to doses of $D = n \times 10^{15} cm^{-2}$ with n =1,2,3,4,5 and 6. The estimated defect concentration corresponding to these doses is n_d=0.1 %, 0.2%, 0.3%, 0.42%, 0.53% and 0.63% respectively. This value is derived as

follows: according to numerical calculations[61, 97], only 0.4% of incident helium ions interact with carbon atoms. Therefore, for each He+ dose, the defects concentration n_d is given in terms of percentage if one considers graphene lattice carbon atoms density $n_C = 3.8 \times 10^{15} cm^{-2}$.
Raman spectroscopy (Renishaw inVia) was performed on samples using freshly exfoliated graphene flakes which were subjected to the same doses as above. The laser excitation wavelength used was 532 nm (i.e. 2.3 eV). The Raman spectra were reproduced several times on the same samples where the ID/IG was roughly similar, therefore no further defects were created or annealed during Raman exposure.
The XPS was performed on a freshly transferred CVD graphene onto Si/SiO_2 substrate (see supporting information), using a Theta Probe Angle-Resolved X-ray Photoelectron Spectrometer, from Thermo Scientific^{TM}. The system uses a Monochromated, Micro-focused Al K-Alpha source delivering a spot size between 15 μm and 400 μm. For our samples a spot size of 100 μm was chosen for optimum measurements.

References

[1] Novoselov, K. S.; Geim, A. K. ; Morozov, S. V.; Jiang, D.; Zhang, Y.; Dubonos, S. V.; Grigorieva, I. V.; Firsov, A. A. Electric Field Effect in Atomically Thin Carbon Films. Science 2004, 306, 666–669.

[2] http://www.itrs.net/

[3] Tan, Y. -W.; Zhang, Y.; Bolotin, K.; Zhao, Y.; Adam, S.; Hwang, E. H. ; Sarma Das, S.; Stormer, H. L.; Kim, P. Measurement of Scattering Rate and Minimum Conductivity in Graphene. Phys. Rev. Lett. 2007, 99, 246803.

[4] Adam, S.; Hwang, E. H.; Galitski, V. M.; Das Sarma, S. A self-consistent theory for graphene transport. PNAS, 2007, 104, 18392–18397.

[5] Das Sarma,S.; Adam, S.; Hwang, E. H.; Enrico, R. Electronic Transport in Two-dimensional Graphene. Rev. Mod. Phys. 2011, 83, 407.

[6] Craciun, M. F.; Khrapach, I.; Barnes, M. D.; Russo, S. Properties and applications of chemically functionalized graphene. J. Phys. Condens. Matter 2013, 25, 423201

[7] Withers, F.; Bointon, T. H.; Dubois, M.; Russo, S.; Craciun, M. F. Nanopatterning of Fluorinated Graphene by Electron Beam Irradiation. Nano Lett. 2011, 11, 3912–3916.

[8] Hong, X.; Cheng, S.-H.; Herding, C.; Zhu, J. Colossal Negative Magnetoresistance in Dilute Fluorinated Graphene. Phys. Rev. B 2011, 83, 085410.

[9] Leenaerts, O.; Peelaers, H.; Hernndez-Nieves, A. D.; Partoens, B.; Peeters, F. M. First-Principles Investigation of Graphene Fluoride and Graphane. Phys. Rev. B 2010, 82, 195436.

[10] Nair, R. R.; Ren, W.; Jalil, R.; Riaz, I.; Kravets, V. G.; Britnell, L.; Blake, P.; Schedin, F.; Mayorov, A. S.; Yuan, S.; et al. Fluorographene: A Two-Dimensional Counterpart of Teflon. Small 2010, 6, 2877–2884

[11] Cheng, S.-H.; Zou, K.; Okino, F.; Gutierrez, H. R.; Gupta, A.; Shen, N.; Eklund, P. C.; Sofo, J. O.; Zhu, J. Reversible Fluorination of Graphene: Evidence of a Two-Dimensional Wide Bandgap Semiconductor. Phys. Rev. B 2010, 81, 205435.

[12] Withers, F.; Dubois, M.; Savchenko, A. K. Electron Properties of Fluorinated Single-Layer Graphene Transistors. Phys. Rev. B 2010, 82, 073403.

[13] Lee, W. H.; Suk, J. W.; Chou, H.; Lee, J.; Hao, Y.; Wu, Y.; Piner, R.; Akinwande, D.; Kim, K. S.; Ruoff, R. S. Selective-Area Fluorination of Graphene with Fluoropolymer and Laser Irradiation. Nano Lett. 2012, 12, 2374–2378.

[14] Elias, D. C.; Nair, R. R.; Mohiuddin, T. M. G.; Morozov, S. V.; Blake, P.; Halsall, M. P.; Ferrari, A. C.; Boukhvalov, D. W.; Katsnelson, M. I.; Geim, A. K.et al. Control of Graphene's Properties by Reversible Hydrogenation: Evidence for Graphane. Science 2009, 323, 610–613.

[15] Balog, B.; Jørgensen, B.; Nilsson, L.; Andersen, M.; Rienks, E.; Bianchi, M.; Fanetti, M.; Lægsgaard, E.; Baraldi, A.; Lizzit, S.; Sljivancanin, Z.; Besenbacher, F.; Hammer, B.; Pedersen, T. G.; Hofmann, P.; Hornekær, L.; Bandgap opening in graphene induced by patterned hydrogen adsorption. Nat. Mat. 2010, 9, 315–319.

[16] Haberer, D.; Vyalikh, D. V.; Taioli, S.; Dora, B.; Farjam, M.; Fink, J.; Marchenko, D.; Pichler, T.; Ziegler, K.; Simonucci, S. Tunable Band Gap in Hydrogenated Quasi-Free-Standing Graphene. Nano Lett. 2010, 10, 3360–3366.

[17] Lu, Y. H.; Wu, R. Q.; Shen, L.; Yang, M.; Sha, Z. D.; Cai, Y. Q.; He, P. M.; Feng, Y. P. Effects of Edge Passivation by Hydrogen on Electronic Structure of Armchair Graphene Nanoribbon and Band Gap Engineering. Appl. Phys. Lett. 2009, 94, 122111.

[18] Choe, D. -H.; Bang, J.; Chang. K. J. Electronic structure and transport properties of hydrogenated graphene and graphene nanoribbons. New J. Phys. 2010 12 125005.

[19] , Chuang, C.; Puddy, R. K.; Lin, H.-D.; Lo, S.-T.; Chen, T.-M.; Smith, C. G.; Liang, C.-T. Experimental Evidence for Efros-Shklovskii Variable Range Hopping in Hydrogenated Graphene. Solid State Commun. 2012, 152, 905–908.

[20] Sofo, J. O.; Chaudhari, A. S.; Barber, G. D. Graphane: A Two-Dimensional Hydrocarbon. Phys. Rev. B 2007, 75, 153401.

[21] Ryu, S.; Han, M. Y.; Maultzsch, J.; Heinz, T. F.; Kim, P.; Steigerwald, M. L.; Brus, L. E. Reversible Basal Plane Hydrogenation of Graphene. Nano Lett. 2008, 8, 4597–4602.

[22] Choe, D.-H.; Chang, K. J. Effect of dimensionality on the localization behavior in hydrogenated graphene systems. Nano Lett., 2012, 12 (10), 5175–5180.

[23] Matis, B. R.; Burgess, J. S.; Bulat, F. A.; Friedman, A. L.; Houston, B. H.; Baldwin, J. W. Surface Doping and Band Gap Tunability in Hydrogenated Graphene. ACS Nano 2012, 6, 17–22.

[24] Havu, P.; Ijäs, M.; Harju, A. Hydrogenated Graphene on Silicon Dioxide Surfaces. Phys. Rev. B 2011, 84, 205423.

[25] Bostwick, A.; McChesney, J. L.; Emtsev, K. V.; Seyller, T.; Horn, K.; Kevan, S. D.; Rotenberg, E.Quasiparticle Transformation during a Metal-Insulator Transition in Graphene. Phys. Rev. Lett. 2009, 103, 056404.

[26] Bang, J.; Chang, K. J. Localization and One-Parameter Scaling in Hydrogenated Graphene. Phys. Rev. B 2010, 81, 193412.

[27] Masubuchi, S.; Arai, M.; Machida, T. Atomic Force Microscopy Based Tunable Local Anodic Oxidation of Graphene. Nano Lett. 2011, 11, 4542–4546.

[28] Seo, S.; Yoon, Y.; Lee, J.; Park, Y.; Lee, H. Nitrogen-Doped Partially Reduced Graphene Oxide Rewritable Nonvolatile Memory. ACS Nano, 2013, 7 (4), 3607–3615.

[29] Wu, X.; Sprinkle, M.; Li, X.; Ming, F.; Berger, C.; de Heer, W. A. Epitaxial-Graphene/Graphene-Oxide Junction: An Essential Step towards Epitaxial Graphene Electronics. Phys. Rev. Lett. 2008, 101, 026801.

[30] Guo, L.; Shao, R.-Q.; Zhang, Y.-L.; Jiang, H.-B.; Li, X.-B.; Xie, S.-Y.; Xu, B.-B.; Chen, Q.-D.; Song, J.-F.; -Sun, H.-B. Bandgap Tailoring and Synchronous Microdevices Patterning of Graphene Oxides. J. Phys. Chem. C 2012, 116, 3594–3599.

[31] Gómez-Navarro, C.; Weitz, R. T.; Bittner, A. M.; Scolari, M.; Mews, A.; Burghard, M.; Kern, K. Electronic Transport Properties of Individual Chemically Reduced Graphene Oxide Sheets. Nano Lett. 2007, 7, 3499–3503.

[32] Fujii, S.; Enoki, T. Cutting of Oxidized Graphene into Nanosized Pieces. J. Am. Chem. Soc. 2010, 132, 10034–10041.

[33] Yan, J.-A.; Xian, L.; Chou, M. Y. Structural and Electronic Properties of Oxidized Graphene. Phys. Rev. Lett. 2009, 103, 086802.

[34] Şahin, H.; Ciraci, S. Chlorine Adsorption on Graphene: Chlorographene. J. Phys. Chem. C 2012, 116, 24075–24083.

[35] Zhang, X.; Hsu, A.; Wang, H.; Song, Y.; Kong, J.; Dresselhaus, M. S.; Palacios, T. Impact of Chlorine Functionalization on High-Mobility Chemical Vapor Deposition Grown Graphene. ACS Nano, 2013, 7 (8), 7262–7270.

[36] Li, B.; Zhou, L.; Wu, D.; Peng, H.; Yan, K.; Zhou, Y.; Liu, Z. Photochemical Chlorination of Graphene. ACS Nano 2011, 5, 5957–5961

[37] Vinogradov, N. A.; Simonov, K. A.; Generalov, A. V.; Vinogradov, A. S.; Vyalikh, D. V.; Laubschat, C.; Mårtensson, N.; Preobrajenski, A. B. Controllable P-Doping of Graphene on Ir(111) by Chlorination with $FeCl_3$. J. Phys.: Condens. Matter. 2012, 24, 314202.

[38] Yang, M.; Zhou, L.; Wang, J.; Liu, Z.; Liu, Z. Evolutionary Chlorination of Graphene: From Charge-Transfer Complex to Covalent Bonding and Nonbonding. J. Phys. Chem. C 2012, 116, 844–850.

[39] Ijäs, M.; Havu, P.; Harju, A. Fracturing Graphene by Chlorination: A Theoretical Viewpoint. Phys. Rev. B 2012, 85, 035440.

[40] Wu, J.; Xie, L.; Li, Y.; Wang, H.; Ouyang, Y.; Guo, J.; Dai, H. Controlled Chlorine Plasma reaction for Noninvasive Graphene Doping. J. Am. Chem. Soc. 2011, 133, 19668–19671.

[41] Englert, J. M.; Dotzer, C.; Yang, G.; Schmid, M.; Papp, C.; Gottfried, J. M.; Steinrck, H.-P.; Spiecker, E.; Hauke, F.; Hirsch, A. Covalent Bulk Functionalization of Graphene. Nat. Chem. 2011, 3, 279–286.

[42] Usachov, D.; Vilkov, O.; Grüneis, A.; Haberer, D.; Fedorov, A.; Adamchuk, V. K.; Preobrajenski, A. B.; Dudin, P.; Barinov, A.; Oehzelt, M.; Laubschat, C.; Vyalikh, D. V. Nitrogen-Doped Graphene: Efficient Growth, Structure, and Electronic Properties. Nano Lett 2011, 11 (12), 5401–5407.

[43] Liu, H.; Lee, J. Y. Electric Field Effects on the Adsorption of CO on a Graphene Nanodot and the Healing Mechanism of a Vacancy in a Graphene Nanodot. J. Phys. Chem. C 2012, 116, 3034–3038.

[44] Hirsch, A.; Englert, J. M.; Hauke, F. Wet Chemical Functionalization of Graphene. Acc. Chem. Res. 2013, 46 (1), 87–96.

[45] Sun, J. T.; Lu, Y. H.; Chen, W.; Feng, Y. P.; Wee, A. T. S. Linear Tuning of Charge Carriers in Graphene by Organic Molecules and Charge-Transfer Complexes. Phys. Rev. B 2010, 81, 155403.

[46] Georgakilas, V.; Otyepka, M.; , Bourlinos, A. B; Chandra, V.; Kim, N.; Kemp, K. C.; Hobza, P.; Zboril, R.; Kim K. S. Functionalization of Graphene: Covalent and Non-Covalent Approaches, Derivatives and Applications. Chem. Rev. 2012, 112 (11), 6156–6214.

[47] Niyogi, S.; Bekyarova, E.; Itkis, M. E.; Zhang, H.; Shepperd, K.; Hicks, J.; Sprinkle, M.; Berger, C.; Lau, C. N.; deHeer, W. A. et al. Spectroscopy of Covalently Functionalized Graphene. Nano Lett. 2010, 10, 4061–4066.

[48] Joucken, F.; Tison, Y.; Lagoute, J.; Dumont, J.; Cabosart, D.; Zheng, B.; Repain, V.; Chacon, C.; Girard, Y.; Botello-Mndez, A. R. et al. Localized State and Charge Transfer in Nitrogen-Doped Graphene. Phys. Rev. B 2012, 85, 161408.

[49] Zhang, H.; Bekyarova, E.; Huang, J.-W.; Zhao, Z.; Bao, W.; Wang, F.; Haddon, R. C.; Lau, C. N. Aryl Functionalization as a Route to Band Gap Engineering in Single Layer Graphene Devices. Nano Lett. 2011, 11, 4047–4051.

[50] Suzuura, H.; Ando, T. Anderson Localization in a Graphene Sheet. J.Phys. Soc. Jpn. 2003, 72, 69–70.

[51] Xu, G.; Torres Jr., C. M.; Tang, J.; Bai, J.; Song, E. B.; Huang, Y.; Duan, X.; Zhang, Y.; Wang, K. L. Edge Effect on Resistance Scaling Rules in Graphene Nanostructures. Nano Lett., 2011,11 (3), 1082–1086.

[52] Kotakoski, J; Krasheninnikov, A. V.; Kaiser, U.; Meyer, J. C. From Point Defects in Graphene to Two-Dimensional Amorphous Carbon. Phys. Rev. Lett. 2011, 106, 105505.

[53] Zhou, Y.-B. ; Liao, Z.-M.; Wang, Y.-F; Duesberg, G. S.; Xu, J.; Fu, Q.; Wu, X.-S.; Yu, D.-P. Ion irradiation induced structural and electrical transition in graphene. J. Chem. Phys. 2010, 133, 234703.

[54] McCann, E; Kechedzhi, K; Falko, V. I.; Suzuura, H.; Ando, T.; Altshuler, B. L. Weak-localization magnetoresistance and valley symmetry in graphene. Phys. Rev. Lett. 2006, 97,146805.

[55] Louis, E; Vergs, J. A. ; Guinea, F.; Chiappe, G. Transport regimes in surface disordered graphene sheets. Phys. Rev. B 2007, 75, 085440.

[56] Lherbier, A.; Biel, B.; Niquet, Y.-M.; Roche, S. Transport Length Scales in Disordered Graphene-Based Materials: Strong Localization Regimes and Dimensionality Effects. Phys. Rev. Lett. 2008, 100, 036803.

[57] Aleiner, I. L.; Efetov, K. B. Effect of disorder on transport in graphene. Phys. Rev. Lett. 2006, 97, 236801.

[58] Gunlycke, D; Areshkin, D. A. ; White, C. T. Semiconducting graphene nanostrips with edge disorder. Appl. Phys. Lett. 2007, 90, 142104.

[59] Ponomarenko, L. A. ; Geim, A. K. ; Zhukov,A. A.; Jalil, R; Morozov, S. V. ; Novoselov, K. S. ; Grigorieva, I. V.; Hill, E. H. ; Cheianov, V. V. ; Fal'ko, V. I. ; Watanabe, K.; Taniguchi, T.; Gorbachev R. V. Tunable metal-insulator transition in double-layer graphene heterostructures. Nat. Phys. 2001, 7, 958–961.

[60] Evaldsson, M; Zozoulenko, I. V.; Xu, H.; Heinzel, T. Edge-disorder-induced Anderson localization and conduction gap in graphene nanoribbons. Phys. Rev. B 2008, 78, 161407(R).

[61] Nakaharai, S.; Iijima, T.; Ogawa, S.; Suzuki, S.; Li, S.-L.; Tsukagoshi, K.; Sato, S.; Yokoyama, N. Conduction Tuning of Graphene Based on Defect-Induced Localization. ACS Nano, 2013, 7 (7), 569–5700.

[62] Tuan, D. V.; Kumar, A; Roche, S.; Ortmann, F.; Thorpe, M. F.; Ordejon P. Insulating behavior of an amorphous graphene membrane. Phys. Rev. B 2012, 86, 121408(R).

[63] Zhang, Y.; Tang, T.; Girit, C.; Hao, Z.; Martin, M.; Zettl, A.; Crommie, M.; Shen, Y.; Wang, F. Direct observation of a widely tunable bandgap in bilayer grapheme. Nature 2009, 459, 820.

[64] Khodkov, T.; Withers, F.; Hudson, D.; Craciun, M.; Russo, S Electrical transport in suspended and double gated trilayer graphene, Appl. Phys. Lett. 2012, 100, 013114.

[65] Lucchese, M; Stavale, F; Ferreira, E. M.;Vilani, C.; Moutinho, M; Achete, R. B. C. C. and Jorio, A. Quantifying ion-induced defects and Raman relaxation length in graphene. Carbon 2010, 48, 1592–1597.

[66] Cançado, L. G.; Jorio, A.; Martins Ferreira, E. H.; Stavale, F; Achete, C. A.; Capaz, R. B.; Moutinho, M. V. O.; Lombardo, A.; Kulmala, T. S.; Ferrari, A. C. Quantifying Defects in Graphene via Raman Spectroscopy at Different Excitation Energies. Nano Lett., 2011, 11 (8), 3190–3196.

[67] Eckmann, A; Felten, A; Mishchenko, A; Britnell, L; Krupke, R; Novoselov, K. S.; Casiraghi, C. Probing the Nature of Defects in Graphene by Raman Spectroscopy. Nano Lett. 2012, 12, 3925–3930.

[68] Eckmann, A; Felten, A; Verzhbitskiy, I; Davey, R.; Casiraghi, C. Raman study on defective graphene: Effect of the excitation energy, type, and amount of defects. Phys. Rev. B 2013, 88, 035426.

[69] Hang, S.; Moktadir, Z.; Mizuta, H. Raman study of damage extent in graphene nanostructures carved by high energy helium ion beam. Carbon 2013, 72, 233.

[70] Withers, F.; Russo, S.; Dubois, M.; Craciun, M. Tuning the electronic transport properties of graphene through functionalisation with fluorine. Nanoscale Research Lett. 2011, 6, 526.

[71] Venezuela, P; Lazzeri, M.; Mauri, F. Theory of double-resonant Raman spectra in graphene: Intensity and line shape of defect-induced and two-phonon bands. Phys. Rev. B. 2011, 84, 035433.

[72] Speranza, G.; Minati, L.; Anderle, M. The C1s core line in irradiated graphite. J. Appl. Phys. 2007, 102, 043504.

[73] Emtsev, K. V.; Speck, F.; Seyller, Th.; Ley, L.; Riley, J. D.; Interaction, growth, and ordering of epitaxial graphene on SiC0001 surfaces: A comparative photoelectron spectroscopy study. Phys. Rev. B 2008, 77, 155303.

[74] Haberer, D.; Giusca, C. E.; Wang, Y.; Sachdev, H.; Fedorov, A. V.; Farjam, M.; Jafari, S. A.; Vyalikh, D. V.; Usachov, D.; Liu, X.; Treske, U.; Grobosch, M.; Vilkov, O.; Adamchuk, V. K.; Irle, S.; Silva, S. R. P.; Knupfer, M.; Bchner, B.; Grneis, A. Evidence for a New Two-Dimensional C_4H-Type Polymer Based on Hydrogenated Graphene. Adv. Mater. 2011, 23, 4497–4503.

[75] Zhou, S. Y.; Gweon, G. H.; Fedorov, A. V.; First, P. N.; de Heer, W. A.; Lee, D. H.; Guinea, F.; Castro Neto, A. H.; Lanzara, A. Substrate-induced bandgap opening in epitaxial graphene. Nat. Mater. 2007, 6, 770–775.

[76] Lizzit, S.; Zampieri, G.; Petaccia, L.; Larciprete, R.; Lacovig, P.; Rienks, E. D. L.; Bihlmayer, G.; Baraldi, A.; Hofmann, P. Manifestation of carbon 1s binding-energy variations in individual X-ray photoemission spectra. Nat. Phys. 2010, 6, 345–349.

[77] Dreyer, D. R.; Park, S.; Bielawski C. W.; Ruoff, R. S. The chemistry of graphene oxide. Chem. Soc. Rev. 2010, 39, 228–240.

[78] Hong, S. K.; Song, S. M.; Sul, O; Choz, B. J. Carboxylic Group as the Origin of Electrical Performance Degradation during the Transfer Process of CVD Growth Graphene. J. Electrochem. Soc. 2012, 159, K107–K109.

[79] Islam, M. R.; Joung, D.; Khondake, S. I. Schottky diode via dielectrophoretic assembly of reduced graphene oxide sheets between dissimilar metal contacts. New J. Phys. 2011, 13, 035021.

[80] Xu, Z.; Che, L.; Li, J.; Wang, R.; Qian, X.; Song, X.; Liu L.; Chen, G. Oxidation and disorder in few-layered graphene induced by the electron-beam irradiation. Appl. Phys. Lett. 2011, 98, 183112.

[81] Jackson, S. T.; Nuzzo, R. G. Determining hybridization differences for amorphous carbon from the XPS C 1s envelope. Appl. Surf. Sci. 1995, 90, 195–203

[82] Mezzi A.; Kaciulis, S.; Surf. Surface investigation of carbon films: from diamond to graphite. Surf. Interface Anal. 2010, 42, 1082–1084.

[83] Susi, T.; Kaukonen, M.; Havu, P.; Ljungberg, M. P.; Ayala P.; Kauppinen, E. I. Beilstein J. Nanotechnol. Core level binding energies of functionalized and defective graphene. 2014, 5, 121.

[84] Robinson, J. P.; Henning, S.; Oroszlány, L; Fal'ko, V. I. Adsorbate-Limited Conductivity of Graphene. Phys. Rev. Lett. 2008, 101, 196803.

[85] Ma, J.; Alfè, D.; Michaelides, A.; Wang E. Stone-Wales defects in graphene and other planar sp^2-bonded materials. Phys. Rev. B 2009, 80, 033407.

[86] Guinea, F.; Katsnelson, M. I.; Vozmediano, M. A. H. Midgap states and charge inhomogeneities in corrugated graphene. Phys. Rev. B 2008, 77, 075422.

[87] Wehling, T. O.; Katsnelson, M. I.; Lichtenstein, A. I. Impurities on graphene: Midgap states and migration barriers. Phys. Rev. B 2009, 80, 085428.

[88] Wehling, T. O.; Balatsky, A. V.; Tsvelik, A. M.; Katsnelson, M. I.; Lichtenstein, A. I. Midgap states in corrugated graphene: Ab initio calculations and effective field theory. Eur. Phys. Lett. 2008, 84, 17003.

[89] Wehling, T. O.; Katsnelson, M. I.; Lichtenstein, A. I. Adsorbates on graphene: Impurity states and electron scattering. Chem. Phys. Lett. 2009, 476, 125–134.

[90] Pereira, V. M.; Lopes dos Santos, J. M. B.; Castro Neto, A. H. Modeling disorder in graphene. Phys. Rev. B 2008, 77, 115109.

[91] Cresti, A.; Ortmann, F.; Louvet, T.; Tuan, D. V.; Roche, S. Broken Symmetries, Zero-Energy Modes, and Quantum Transport in Disordered Graphene: From Supermetallic to Insulating Regimes. Phys. Rev. Lett. 2013, 110, 196601.

[92] Manoharan, M.; Mizuta, H. Point-defect induced transport bandgap widening in the downscaled armchair graphene nanoribbon device. Carbon 2013, 64, 416.

[93] Hiura, H.; Miyazaki, H.; Tsukagoshi, K. Determination of the Number of Graphene Layers: Discrete Distribution of the Secondary Electron Intensity Stemming from Individual Graphene Layers. Appl. Phys. Exp. 2010, 3, 095101.

[94] Ferrari, A. C. ; Meyer, J. C. ; Scardaci, V.; Casiraghi, C.; Lazzeri, M; Mauri , F.; Piscanec, S; Jiang, D; Novoselov, K. S. ; Roth, S.; Geim, A. K. Raman spectrum of graphene and graphene layers. Phys. Rev. Lett. 2006, 97, 187401.

[95] Boden, S. A. ; Moktadir, Z. ; Bagnall, D. M. ; Mizuta, H.; Rutt H. N. Focused helium ion beam milling and deposition. Microelectron. Eng. 2011, 88, 2452–2455.

[96] Lemme , M. C. ; Bell, D. C. ; Williams, J. R; Stern , L. A.; Baugher , B. W. H. ; Jarillo-Herrero, P. ; and Marcus C. M. Etching of Graphene Devices with a Helium Ion Beam. ACS Nano 2009, 3 , 2674–2676.

[97] Bell, D. C. ; Lemme, M. C. ; Stern, L. A. ; Williams, J. R. ; Marcus C. M. Precision cutting and patterning of graphene with helium ions. Nanotechnology 2009, 20 , 455301.

[98] Fox, D; Zhou, Y. B. ; O'Neill, A.; Kumar, S; Wang, J. J. ; Coleman J. N. ; Duesberg, G. S.; Donegan J. F.; Zhang, H. Z., Helium ion microscopy of graphene: beam damage, image quality and edge contrast. Nanotechnology 2013, 24, 335702.

[99] Winston, D.; Cord, B. M. ; Ming, B.; Bell, D. C.; DiNatale, W.F.; Stern, L. A.; Vladar, A. E.; Postek, M. T.; Mondol, M. K.; Yang, J. K. W.; Berggren, K. K. Scanning-helium-ion-beam lithography with hydrogen silsesquioxane resist. J. Vac. Sci. Technol. B Microelectron Nanometer Struct. 2009, 27, 2702.